Journal of Drug Delivery Science and Technology 94 (2024) 105490

Contents lists available at ScienceDirect

Journal of Drug Delivery Science and Technology

journal homepage: www.elsevier.com/locate/jddst

Self-assembling nanoparticles with antioxidant activity for ROS scavenging in liver cells

Valeria Nele, Stefania Melini, Virginia Campani, Alessia Angelillo, Sossio Fabio Graziano, Claudio Pirozzi, Rosaria Meli, Giuseppe De Rosa *

Department of Pharmacy, University of Naples Federico II, Via D. Montesano, 49, 80131, Naples, Italy

ARTICLE INFO

Keywords:
Self-assembling nanoparticles
Cerium oxide
Lipid nanoparticles
Antioxidant activity
ROS scavenging
Liver disease

ABSTRACT

Oxidative stress plays a crucial role in the pathogenesis of hepatic disorders, including non-alcoholic fatty liver disease (NAFLD) and its progression into hepatitis and fibrosis. In this context, the use of nanomaterials with ROS-scavenging activity might be a promising therapeutic approach. Here, we designed lipid self-assembling nanoparticles (SANP) enriched with a cerium core to obtain a ROS-scavenging nanoparticle platform. We optimized the preparation of cerium-doped SANP (Ce-SANP) by tuning the ratios between the various components and characterized the formulations in terms of colloidal properties, stability against aggregation in serum proteins, and capability to scavenge ROS in a hepatocyte model of oxidative stress. Specifically, we identified Ce-SANP formulations with suitable colloidal properties and peroxidase- and superoxide dismutase-like activity. In *in vitro* studies, Ce-SANP showed a marked cytocompatibility and reduced ROS levels counteracting H_2O_2-induced oxidative damage in HepG2 cells. These results indicate the potential antioxidant of the proposed Ce-SANP platform technology in limiting oxidative damage, a key target to hinder the etiopathogenesis and progression of liver diseases.

1. Introduction

Chronic liver diseases are mostly characterized by increased oxidative damage, regardless of the etiopathogenesis of the liver disorder [1]. With a global prevalence of 25%, non-alcoholic fatty liver disease (NAFLD) is one of the most common chronic liver diseases; liver steatosis and its progression in steatohepatitis (NASH) is often associated to the onset of cirrhosis and hepatocellular carcinoma [2]. However, the mechanism of progression from simple fat deposition to NASH is complex, and previous reports have linked NAFLD to several factors including oxidative stress [3]. The continuous accumulation of triglycerides in NAFLD leads to mitochondrial damage and following reactive oxygen species (ROS) release due to altered fatty acid oxidation (FAO) [4]. The development of NASH includes hepatocyte necrosis and sustained inflammatory response [2,5]. Pro-inflammatory mediators released by necrotic hepatocytes induce the *trans*-differentiation of hepatic stellate cells in myofibroblasts which start to deposit abnormal amounts of extracellular matrix components triggering liver fibrosis [2]. Despite the increasing prevalence of NAFLD, there is a lack of clinically approved drugs for this disease [2]; however, several therapeutic strategies aim at reducing ROS levels.

Antioxidant systems consist of enzymatic and non-enzymatic components. The enzymatic system includes superoxide dismutase (SOD), catalase (CAT), and glutathione peroxidase and reductase (GSH-Px) that are responsible for detoxifying ROS. Non-enzymatic compounds include small molecules with antioxidant activity such as flavonoids (*e.g.*, isorhamnetin [6] and silymarin [7]), polyphenols (*e.g.*, resveratrol [8]), vitamins (*e.g.*, ascorbic acid [9]), or ROS-scavenging proteins of the globin family (*i.e.*, cytoglobin, myoglobin, and neuroglobin) [10]. However, the administration of antioxidant agents is often challenging due to their chemical instability, poor water solubility, and bioavailability [11–13]. Nanotechnology-based approaches have been proposed to overcome these limitations for the development of antioxidant therapies [14,15]. In the context of liver diseases, nanoparticles based on materials with intrinsic ROS-scavenging activity, such as cerium oxide, have gained increasing interest for the treatment of NAFLD as evidenced by *in vitro* and *in vivo* studies [16–18].

Otherwise, therapeutic approaches based on the regulation of target genes or proteins by means of coding or non-coding RNA have emerged for the treatment of chronic liver disease [19,20]. However, *in vivo*

* Corresponding author.
E-mail address: gderosa@unina.it (G. De Rosa).

https://doi.org/10.1016/j.jddst.2024.105490
Received 31 October 2023; Received in revised form 7 February 2024; Accepted 18 February 2024
Available online 28 February 2024

delivery of RNA requires the use of vectors to enhance cellular uptake and prevent nuclease degradation of RNA [21]. We have previously developed hybrid self-assembling nanoparticles (SANP) with an inorganic calcium phosphate (CaP) core enclosed by a lipid shell to deliver bisphosphonates [22–25] and nucleic acids [26] to the brain. Lipid SANP formulations have been shown to possess excellent biocompatibility, high nucleic acid encapsulation efficiency and good intracellular delivery. Furthermore, SANP can be assembled by mixing the components at room temperature without the need of complex manufacturing equipment [26]. SANP have been shown to successfully deliver microRNA into the liver [26], although their use in liver pathologies has not been explored yet.

The complexity of the chronic hepatic disorders including NAFLD requires a multi-functional nanoparticle platform able to scavenge ROS and to deliver specific drugs into the liver. In this work, we expanded the capability of our well-established lipid SANP technology by modifying the nanoparticle inorganic core with cerium to confer ROS-scavenging properties to such nanoparticles. We developed a coprecipitation method to produce cerium-doped CaP nanoparticles with varying ratios between the components and characterized these nanoparticles in terms of colloidal properties and antioxidant activity. Then, selected formulations were combined with cationic liposomes to obtain cerium-SANP (Ce-SANP), whose colloidal properties, surface charge, enzymatic activity, and stability against aggregation in the presence of serum albumin were investigated. We carried out cell viability studies on hepatocytes in the presence or not of varying concentrations of Ce-SANP and demonstrated the ability of Ce-SANP formulations to scavenge ROS.

2. Material and methods

2.1. Drugs and chemicals

Sodium chloride (NaCl), calcium chloride ($CaCl_2$), sodium phosphate dibasic (Na_2HPO_4), cerium (III) nitrate, sodium citrate tribasic dihydrate ($C_6H_5Na_3O_7{\cdot}2H_2O$), ammonia solution (28–30%), and the SOD assay kit (cat. n. 19,160) were purchased from Merk Life Science S. r.l. (Milan, Italy). 1,2-dioleoyl-3-trimethylammonium-propane chloride (DOTAP) was kindly donated by Lipoid GmbH (Ludwigshafen, Germany) while *N*-palmitoylsphingosine-1 {succinyl [methoxy (polyethylene glycol) 2000]} (Cer_{16}-PEG_{2000}) was purchased from Avanti Polar Lipids (Alabaster, USA). The 3,3′,5,5′-Tetramethylbenzidine (TMB) substrate solution (cat. n. N301) and the Stop solution (cat. n. N600) were purchased from ThermoFisher Scientific (Rodano, Italy) while regenerated cellulose syringe filters with a 0.2 μm pore size were purchased from Exacta + Optech Labcenter SpA (San Prospero, Italy).

2.2. CaP nanoparticle preparation

The CaP nanoparticles were prepared by the dropwise addition of 2 mL of an aqueous solution containing Na_2HPO_4 at varying concentrations to 2 mL of an aqueous solution containing $CaCl_2$ at varying concentrations and either 50 mM or 100 mM sodium citrate tribasic (Na_3Cit) while vortex stirring at 1400 rpm. The obtained nanoparticle suspension was incubated at 37 °C for 5 min and stored at 4 °C overnight prior to analysis. The concentrations used in this study are reported in Table 1.

Table 1
Concentrations of $CaCl_2$ and Na_2HPO_4 and relative Ca/P ratio used for the formulation of CaP nanoparticles.

$[Na_3Cit]_{pre\text{-}mix}$	$[CaCl_2]_{pre\text{-}mix}$	$[Na_2HPO_4]_{pre\text{-}mix}$	Ca/P ratio
50 or 100 mM	30 mM	45 mM	0.67
100 mM	34 mM	41 mM	0.83
50 or 100 mM	45 mM	30 mM	1.5
100 mM	47 mM	28 mM	1.67

2.3. Cerium-CaP nanoparticle preparation

The inorganic cerium-CaP nanoparticles were prepared by a modified co-precipitation method involving the dropwise addition of 1 mL of an aqueous solution containing 30 mM Na_2HPO_4 to 1 mL of an aqueous solution containing 100 mM sodium citrate tribasic, $CaCl_2$, and Cerium (III) nitrate while vortex stirring at 1400 rpm; 250 μL of 1.4 M NH_4OH solution were then added dropwise while vortex stirring at 1400 rpm. The obtained nanoparticle suspension was incubated at 37 °C for 5 min, stored at 4 °C overnight, and filtered through a 0.22 μm pore-sized RC membrane. The cerium-CaP nanoparticles were stored at 4 °C until further use. The concentrations of $CaCl_2$ and Cerium (III) nitrate as well as the Ca/P and Ce/P ratios used in this study are reported in Table 2.

2.4. Determination of the gravimetric yield of Cerium-CaP nanoparticles

Aliquots of Cerium-CaP nanoparticles were transferred in 2 mL Eppendorf tubes and frozen at −20 °C overnight prior to lyophilization. Lyophilized samples were then weighted and the gravimetric yield was calculated by using the following formula:

$$gravimetric\ yield = \frac{mass\ of\ lyophilized\ sample}{theoretical\ mass} * 100.$$

2.5. Liposome formulation

Liposomes comprising DOTAP (94 mol%) and Cer_{16}-PEG_{2000} (6 mol %) were prepared *via* the thin film hydration method followed by extrusion. The lipids were dissolved in a chloroform:methanol mixture (2:1 v/v) and transferred in a 50 mL round bottom flask in the appropriate ratios. The organic solvent mixture was removed by rotary evaporation (Laborata 4010 digital, Heidolph, Schwabach, Germany), after which the obtained lipid film was hydrated with deionized water for 2 h at 65 °C to a final lipid concentration of 2.5 mg/mL. The vesicles were extruded through pore-sized polycarbonate membranes (Nucleopore Track-Etched 25 mm membrane, Whatman, Brentford, UK) by using a thermobarrel extruder (Lipex Extruder, Evonik, Essen, Germany) at 65 °C. More specifically, the vesicle suspension was forced through 400 nm membranes (3 passages), 200 nm membranes (3 passages), and 100 nm membranes (5 passages).

2.6. Cerium-SANP nanoparticle formulation

Ce-SANP were prepared by mixing the components (inorganic nanoparticles and liposomes) in a 1:1 v/v ratio followed by incubation for 25 min at room temperature.

2.7. Nanoparticle physico-chemical characterization

The formulations were characterized in terms of colloidal dimensions, polydispersity index (PDI), surface charge, and stability against aggregation in water by using dynamic light scattering (DLS) (Zetasizer Nano Z, Malvern, UK). For each formulation the z-average

Table 2
Concentrations of $CaCl_2$ and Cerium (III) nitrate and relative Ca/P and Ce/P ratios used for the formulation of cerium-CaP nanoparticles.

$[CaCl_2]_{pre\text{-}mix}$	$[Ce(III)nitrate]_{pre\text{-}mix}$	Ca/P ratio	Ce/P ratio
20 mM	50 mM	0.67	1.67
25 mM	50 mM	0.83	1.67
45 mM	50 mM	1.5	1.67
50 mM	50 mM	1.67	1.67
20 mM	150 mM	0.67	5
25 mM	150 mM	0.83	5
45 mM	150 mM	1.5	5
50 mM	150 mM	1.67	5

diameter, PDI, and zeta potential were calculated as mean ± standard deviation of measurements from N ≥ 2 independent batches.

2.8. Peroxidase assay

The peroxidase-like activity of Ce–CaP NPs and Ce-SANP was measured according to a previously published protocol [27]. Briefly, 50 μL of the TMB substrate solution were added to each well of a clear 96-well plate and mixed with 50 μL of an aqueous suspension of Ce–CaP NPs or Ce-SANP at 210 μg/mL. The reaction mixture was incubated for 1 min and stopped by the addition of 50 μL of stop solution (0.16 M sulfuric acid). The absorbance was measured on a spectrophotometer (Thermo Scientific™ Multiskan™ GO Microplate Spectrophotometer) at 451 nm.

2.9. Superoxide dismutase (SOD) assay

To probe the SOD-like activity of Ce–CaP NPs and Ce-SANP an SOD assay kit (cat. n. 19,160) was used following the manufacturer's instructions. 10 μL of an aqueous suspension of Ce–CaP NPs or Ce-SANP at 30 μg/mL were added to 100 μL of an aqueous solution containing the substrate (2-(4-iodophenyl)-3-(4-nitrophenyl)-5-(2,4-disulfophenyl)-2*H*-tetrazolium, monosodium salt, WST-1) to each well of a clear 96-well plate. Following this, 10 μL of a xanthine oxidase solution (obtained by diluting 15 μL of xanthine oxidase solution in 2.5 mL of dilution buffer) were then added to each well and the plate was incubated at 37 °C for 20 min. The absorbance was measured at 440 nm by using a GloMax® Discover Microplate Reader (Promega Instruments). 10 μL of DI water were added to wells containing the WST-1 solution and the enzyme solution (Blank 1, full conversion of the WST-1 substrate) or to wells containing the WST-1 solution and the dilution buffer (Blank 2, no conversion) as a control. The SOD activity was calculated by the following equation:

$$SOD\ activity\ \% = \frac{(A_{Blank\ 1} - A_{Blank\ 2}) - A_{sample}}{(A_{Blank\ 1} - A_{Blank\ 2})} * 100,$$

where $A_{Blank\ 1}$, $A_{Blank\ 2}$, and A_{sample} are the measured absorbance values of wells containing the Blank 1, the Blank 3 or the Ce–CaP NPs/Ce-SANP, respectively.

2.10. SEM-EDS analysis of Ce–CaP nanoparticles

Microstructural and microchemical investigations were carried out at the scanning electron microscopy laboratory of the Department of Earth Sciences, Environment and Resources (University of Naples Federico II). The instrument used is a FESEM with EDS (Field Emission Scanning Electron Microscope equipped with an energy dispersive spectrometer) model Zeiss Merlin VP Compact coupled with a microanalysis unit (Oxford Instruments) and an INCA X-Max solid-state detector (Carl-Zeiss). Data sets were evaluated by means of INCA Energy software 5.05 (XPP array and pulse pile-up corrections) with following operative conditions: 15-kV primary beam voltage, 50–100 A filament current, variable spot size, 50 s real-time counting. Signals optimization was carried out by using cobalt (FWHM peak height of the strobed zero = 60–65 eV) as reference along with standard materials from Smithsonian Institute and MAC (Micro-Analysis Consultants Ltd., Saint Ives. UK) for elements calibration. Accuracies about EDS chemical analyses are reported in Ref. [28].

2.11. Cell culture and viability

Human HepG2 cells (American Type Culture Collection, Manassas, VA, USA) were chosen as an appropriate *in vitro* model to test cell viability and oxidative damage in presence or not of Ce–CaP SANP formulations. Cells were cultured in DMEM medium (2 g/L glucose) supplemented with 10% FBS and 1% antibiotics (100 units/mL penicillin and streptomycin) at 37 °C with 5% CO_2. HepG2 cells were seeded in P96-well microtiter plates (2×10^4 cells/well), starved in 2% FBS medium for 6 h, and incubated with Ce–CaP SANP formulations (30–300 μg/mL) or vehicle for 24 h. The reference concentration of the Ce–CaP SANP used for the *in vitro* studies is the mass concentration of Ce–CaP NPs following the preparation of Ce–CaP SANP formulations. The modification of cell viability after 24 h has been evaluated by 3-(4,5-dimethylthiazol-2-yl)-2,5-diphenyltetrazolium bromide (MTT) assay by spectrophotometric measurement (550 nm absorbance).

2.12. Reactive oxygen species (ROS) production assay

HepG2 cells were seeded in P96-well microtiter dark plates (3×10^4 cells/well), and, after reaching the confluence, were starved in 2% FBS medium for 6 h. Then, cells were incubated with a final concentration of 10 μM dichlorofluorescein diacetate (DCFH-DA) (Sigma–Aldrich, Milan, Italy) in dimethyl sulfoxide for 30 min at 37 °C. Cells were washed with phosphate buffer solution and stimulated with *tert*-butyl hydroperoxide (100 μM) plus H_2O_2 (100 μM) for 3 h to induce oxidative damage. Fifteen minutes after pro-oxidant challenge, Ce–CaP SANP formulations (50, 100, and 200 μg/mL) were added to determine their potential ROS scavenging-like activity. The fluorescence measurements were performed with aHTS-7000 Plus plate reader spectrofluorometer (PerkinElmer, Wellesley, MA, USA) at 485 nm for excitation and 525 nm for emission wavelengths. ROS were quantified as percentage vs control unstimulated cells. The reference concentration of the Ce–CaP SANP used for the *in vitro* studies is the mass concentration of Ce–CaP NPs following the preparation of Ce–CaP SANP formulations.

2.13. Statistical analysis

Data are presented as mean value ± SEM for at least three experiments. Statistical analysis was performed by One-way ANOVA followed by Bonferroni's post-hoc, for multiple comparisons. Differences among groups were considered significant at values of $P < 0.05$. Analyses were performed using GraphPad Prism 9 (GraphPad Software, San Diego, CA, USA).

3. Results and discussion

3.1. Preparation of stabilized CaP nanoparticles (CaP NPs)

Due to their high biocompatibility, pH-dependent dissolution behavior and the ability to complex various biomolecules, calcium phosphate nanoparticles (CaP NPs) have been extensively investigated as drug delivery carriers [29,30]. CaP NPs can be obtained by a co-precipitation method based on the rapid mixing of an aqueous solution containing calcium ions with an aqueous solution containing phosphate anions. However, the rapid nucleation and growth of calcium phosphate can result in the formation of large particles with heterogenous size distributions, which makes the use of stabilizers necessary [30]. Examples of stabilizer molecules include sodium citrate [31,32] and polymers such as poly (ethylene glycol)-block-poly (aspartic acid) [33], poly (ethylene glycol) [34], polyvinylpyrrolidone or polyethyleneimine [35], and carboxymethyl cellulose [36]. Here, we chose sodium citrate as a stabilizer molecule for the preparation of CaP NPs given its ability to chelate calcium ions [37] and investigated the effect of the sodium citrate concentration and the calcium:phosphate (Ca/P) ratio on the size of the obtained nanoparticles.

Citrate-doped CaP NPs were prepared by mixing an aqueous solution containing $CaCl_2$ and trisodium citrate with an aqueous Na_2HPO_4 solution at various Ca:P ratios followed by incubation at 37 °C; dynamic light scattering (DLS) was used to characterize the nanoparticles in terms of their colloidal properties. For Ca:P ratios of 0.67 and 1.5, citrate-coated CaP NPs exhibited z-average diameters above 400 nm

when 50 mM trisodium citrate (Na_3Cit) was used; smaller nanoparticles (z-average diameters <80 nm) could be obtained in the presence of 100 mM trisodium citrate (Fig. 1a). The reduction in the CaP NP size with increasing trisodium citrate concentration may be due to the formation of citrate-calcium complexes which prevent the rapid nucleation and precipitation of CaP NPs [38]. At 100 mM trisodium citrate, nanoparticles with a z-average diameter of 160 ± 60 nm could be produced also for a Ca:P ratio of 1.67 whereas larger diameters (580 ± 204 nm) were observed for a Ca:P ratio of 0.83 (Fig. 1b). We therefore chose 100 mM as the concentration of trisodium citrate for subsequent studies.

3.2. Preparation of cerium-modified CaP nanoparticles (Ce–CaP NPs)

Modifications to the CaP NP composition with other ions can be leveraged to provide CaP NPs with additional functionalities; for example, CaP NP doping with manganese, iron, or silver has been proposed for magnetic resonance imaging [39,40] or anti-bacterial applications [41], respectively. In order to endow citrate-stabilized CaP NPs with ROS-scavening properties, we sought to include cerium ions in their composition by modifying the preparation protocol previously developed for CaP NPs. Briefly, we added $Ce(NO_3)_3$ to an aqueous solution containing $CaCl_2$ and 100 mM trisodium citrate, which was subsequently mixed with an aqueous solution of Na_2HPO_4. The Ce–CaP NPs were prepared at Ca:P ratios of 0.67, 0.83, 1.5, and 1.67 and at two cerium:phosphate (Ce:P) ratios, namely 1.67 and 5. The excess of Ce^{3+} is expected to induce the formation of cerium oxide alongside cerium phosphate [42] while sodium citrate is used as a stabilizer to prevent nanoparticle aggregation [43].

DLS measurements revealed that for Ce:P = 1.67 nanoparticles with z-average diameters <10 nm were obtained regardless of the Ca:P ratio used, while for Ce:P = 5 Ca:P ratios of 0.67 and 1.67 yielded nanoparticles with z-average diameters >400 nm and were not used in subsequent studies. Ce–CaP NPs with diameters of 122 ± 3 nm and 136 ± 1 nm and PDI values below 0.25 were produced for Ce:P = 5 and Ca:P ratios of 0.83 and 1.5, respectively (Fig. 2). It is interesting to note that in the absence of cerium ions, a Ca:P ratio of 0.83 yielded nanoparticles with large diameters (> 500 nm) while a Ca:P ratio of 0.67 resulted in the formation of nanoparticles with diameters smaller than 80 nm. These phenomena may be ascribed to complex concentration-dependent interactions occurring between calcium, phosphate, cerium, and citrate ions upon mixing which may affect the final nanoparticle size. It is well known that cerium ions can form coordination complexes with citrate [43] and can react with phosphate anions to form cerium phosphate [42]; similarly, calcium can interact with both citrate and phosphate ions [32].

In order to investigate the effect of the formulation parameters on the final nanoparticle yield, we carried out a gravimetric analysis following sample lyophilization. An increase in the Ce:P ratio from 1.67 to 5 led to a reduction in the nanoparticle yield, with the exception of the formulation prepared with a theoretical Ca:P ratio of 0.83 (Table 3). We also assessed the colloidal stability against aggregation of the Ce–CaP NPs over 21 days when stored at refrigerated temperatures. Ce–CaP NPs prepared with a Ce:P ratio of 1.67 and Ca:P ratios of 1.5 and 1.67 exhibited minimal changes in the z-average diameter, which suggests a good colloidal stability in water, while a gradual increase in size was observed for Ca:P ratios of 0.67 and 0.83 (Fig. 3a). This behavior may be ascribed to the presence of unreacted ions able to adsorb at the nanoparticle surface and drive nanoparticle aggregation. We explored the possibility to lyophilize these formulations and observed minimal variations in the z-average diameter upon reconstitution of the lyophilized formulations in water (Fig. 3b), making lyophilization a suitable strategy to extend their shelf-life.

Ce–CaP NPs formulated with Ce:P = 5 and Ca:P ratio of 0.83 exhibited good stability against aggregation in water, as opposed to Ce–CaP NPs with a Ca:P ratio of 1.5, for which a large change in the z-

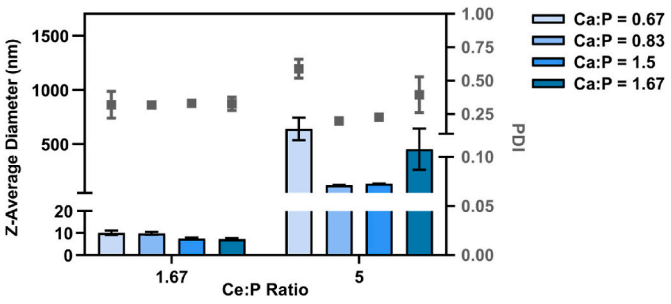

Fig. 2. Z-average diameter (bars) and PDI (square symbols) of CaP NPs prepared with varying Ca:P and Ce:P ratios. Data is reported as mean ± s.d. of N = 3 independent batches.

Table 3
Gravimetric yield of Ce–Ca NPs at varying Ce:P and Ca:P ratios. Values are reported as mean ± s.d. of N = 3 independent batches, with n = 2 technical replicates for each batch.

Ca/P ratio	Ce/P ratio	Gravimetric yield %	Ce/P ratio	Gravimetric yield %
0.67	1.67	56.5 ± 1.4	5	34.9 ± 1.0
0.83	1.67	64.7 ± 0.7	5	57.4 ± 1.5
1.5	1.67	64.6 ± 0.2	5	35.8 ± 5.8
1.67	1.67	56.4 ± 1.3	5	38.8 ± 2.5

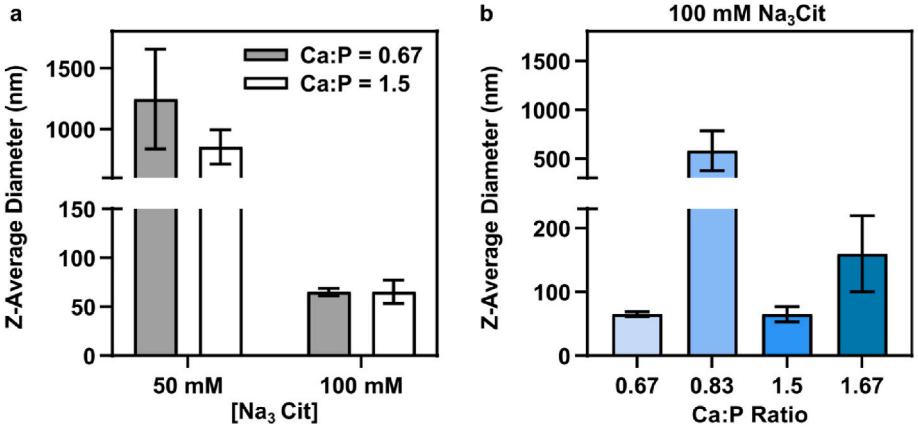

Fig. 1. (a) Z-average diameter of CaP NPs prepared with 50 mM or 100 mM trisodium citrate and Ca:P ratios of 0.67 and 1.5. (b) Z-average diameter of CaP NPs prepared with 100 mM trisodium citrate and varying Ca:P ratios. Data is shown as mean ± s.d. of N = 3 independent batches.

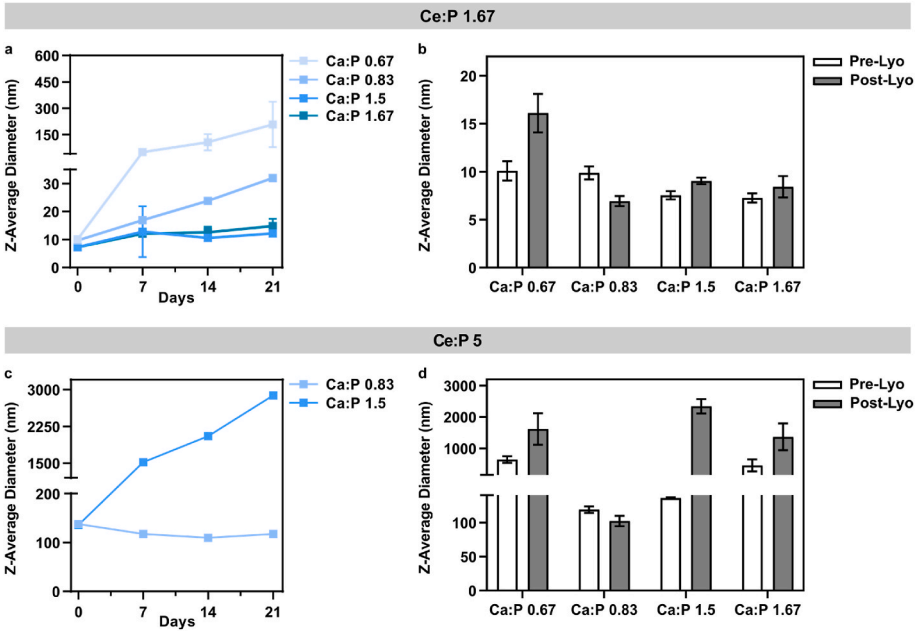

Fig. 3. Z-average diameter and PDI of Ce–CaP NPs with varying Ca:P ratios and Ce:P = 1.67 (a) or Ce:P = 5 (c) at 4 °C over 21 days and pre- and post-lyophilization (b,d). Data is shown as mean ± standard deviation of N ≥ 2 independent batches.

average diameter was observed (Fig. 3c). Reconstitution of the lyophilized formulations resulted in a further increase in the colloidal dimension of Ce–CaP NPs with Ce:P = 5 and Ca:P ratios of 0.67, 1.5, and 1.67 (Fig. 3d), which were excluded from subsequent studies.

3.3. Enzyme-like activity and SEM-EDS analysis of Ce–CaP nanoparticles

Cerium-based nanomaterials have been shown to mimic the activity of ROS-scavenging enzymes such as peroxidase and SOD, which may be due to a redox cycle of Ce^{3+} and Ce^{4+} and the presence of oxygen vacancies at nanoparticle surface [44]. We probed the peroxidase-like activity of the Ce–CaP NPs by a colorimetric assay based on the redox reaction between 3,3′,5,5′-Tetramethylbenzidine (TMB) and H_2O_2 as previously reported [45,46]. In the presence of Ce–CaP NPs and H_2O_2, TMB is converted in a blue-colored product with absorption peaks at 370 and 653 nm; the reaction can be stopped by the addition of 0.16 M sulfuric acid solution ("stop solution"), which forms a yellow diamine compound with a characteristic absorption peak at 451 nm [46]. Ce–CaP NPs with a Ce:P ratio of 5 and a Ca:P ratio of 0.83 exhibited the highest peroxidase-like activity, which markedly decreased for a Ca:P ratio of 1.5; a lower Ce:P ratio resulted in a reduction in the peroxidase-like activity (Fig. 4a), as previously reported for cerium phosphate-cerium oxide nanocomposites [42].

Next, we assessed the SOD-like activity of Ce–CaP NPs with a colorimetric assay based on the formation of a formazan dye with an absorption peak at 450 nm following the oxidation of a water-soluble tetrazolium salt by superoxide anions generated by xanthine oxidase. A decrease in the concentration of the dye can be observed in the presence of SOD which converts the superoxide anion into hydrogen peroxide and oxygen [47]. Ce–CaP NPs with a Ca:P ratio of 0.83 and a Ce:P ratio of 5 exhibited the highest SOD-like activity (61.9 ± 1.4 %), which was higher than 56% also for the Ce–CaP NPs prepared with a Ce:P ratio of 1.67 and Ca:P ratios of 0.67 and 1.67 (Fig. 4b). No SOD-like activity could be detected for Ce–CaP NPs with a Ce:P ratio of 5 and a Ca:P ratio of 1.5. The observed differences in the Ce–CaP NPs peroxidase- and SOD-like activity with varying Ce:P and Ca:P ratios may be due to variations in the structure and surface composition of the nanoparticles. Overall, these findings indicated that some of the screened Ce–CaP NP formulations could work as peroxidase and SOD mimics. Based on the results of the enzymatic activity assays, we selected the formulations with a Ce:P ratio of 5 (Ca:P ratio = 0.83) and Ce:P ratio of 1.67 (Ca:P ratios = 0.67 and 1.67) for the next part of the study.

We carried out SEM-EDX analysis to investigate the structural and compositional features of the Ce–CaP NPs selected from the enzymatic activity assays (Ce:P ratio of 5 with a Ca:P ratio of 0.83 and Ce:P ratio of 1.67 with Ca:P ratio of 0.67 and 1.67). Two nanoparticle populations with subspherical morphology and sizes <50 nm or >100 nm were identified *via* SEM for all the investigated samples. The differences in the nanoparticle size measured by SEM and DLS may be due to nanoparticle aggregation in water, as previously reported for titanium oxide

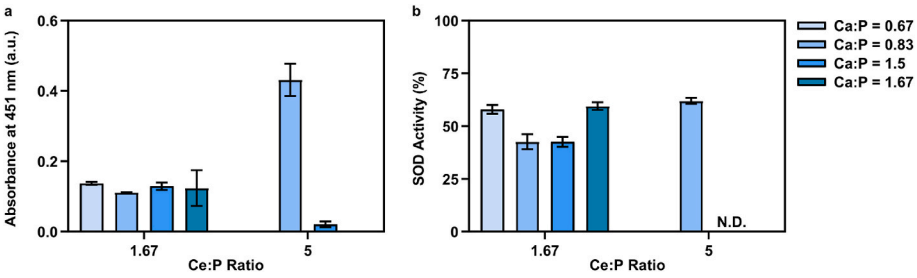

Fig. 4. (a) Peroxidase-like activity of Ce–CaP NPs with varying Ca:P and Ce:P ratios at 105 μg/mL (b) SOD-like activity of Ce–CaP NPs with varying Ca:P and Ce:P ratios at 25 μg/mL. Data is reported as mean ± s.d. of N = 2–3 independent batches with n = 3 technical replicates.

nanoparticles [48]. Image analysis revealed that nanoparticles with sizes <50 nm represented at least 90% of the total while nanoparticles with sizes >100 nm represented the 5–10% of the total (Supplementary Figs. S1–3).

The chemical composition of the nanoparticles was investigated by EDS analysis (Supplementary Table S1), from which nanoparticle formulations with a Ce:P ratio of 5 (Ca:P ratio of 0.83) or a Ce:P ratio of 1.67 (Ca:P ratio of 1.67) had a cerium content between 31 and 36%. Nanoparticle formulations with a Ce:P ratio of 1.67 and a Ca:P ratio of 0.67 exhibited higher cerium content (49%). From the semi-quantitative EDS analysis we cannot exclude that upon dissolution of the precursor salts Ce^{3+}, PO_4^{3-}, and Ca^{2+} form insoluble salts such as cerium phosphate and calcium phosphate which precipitate as Ce–CaP NPs; the remaining cerium may form cerium oxide [42]. It is worth mentioning that the low signal for calcium and phosphorus is likely to be due to the Au metallization used for sample preparation for SEM.

3.4. Formulation and characterization of Ce-SANP

Various organic materials have been used to coat cerium-based nanomaterials to improve nanoparticle serum stability against aggregation and cellular uptake, as well as to provide a handle for surface functionalization [49–54]. We investigated whether it was possible to form SANP by mixing Ce–CaP NPs with DOTAP:CerPEG liposomes to obtain cerium-doped SANP (Ce-SANP). The liposomes had a z-average diameter of 128 ± 2 nm, a PDI of 0.09 ± 0.02, and a zeta potential of +61 ± 3.5 mV. Mixing and incubation of the liposomes with the Ce–CaP NPs selected in the first part of the study yielded SANP with z-average diameters <150 nm and a PDI <0.2 (Fig. 5b); the Ce-SANP formulations were negatively charged, with zeta potentials < −35 mV (Fig. 5c). The resulting hydrodynamic diameter and surface charge of Ce-SANP formulations differed from those of the liposomes and may be indicative of structural reorganization of the components upon mixing as previously reported [55].

Then, we evaluated the peroxidase- and SOD-like activity of Ce-SANP formulations to assess whether they retained the enzyme-like activity of bare Ce–CaP NPs. In analogy to what we observed for the Ce–CaP NPs, the Ce-SANP exhibited similar peroxidase-like activity (Fig. 5d) and SOD-like activity (Fig. 5e) to bare Ce–CaP NPs, which suggests that these nanoparticle formulations could be used for ROS scavenging applications. The enzyme-like properties of Ce–CaP NP formulations were not influenced by the presence of the lipid coating, as previously reported [56].

In order to assess the colloidal stability of Ce-SANP formulations in biological fluids, we incubated the formulations for 4 h at 37 °C in a 1 w/v % BSA solution. The mean hydrodynamic diameter of the Ce-SANP formulations was measured *via* DLS at T_0, 30 min and 4 h post-incubation in an aqueous BSA solution; nanoparticles diluted in a 150 mM NaCl solution were used as a positive control. A large increase in the hydrodynamic diameter was observed for Ce-SANP obtained by mixing

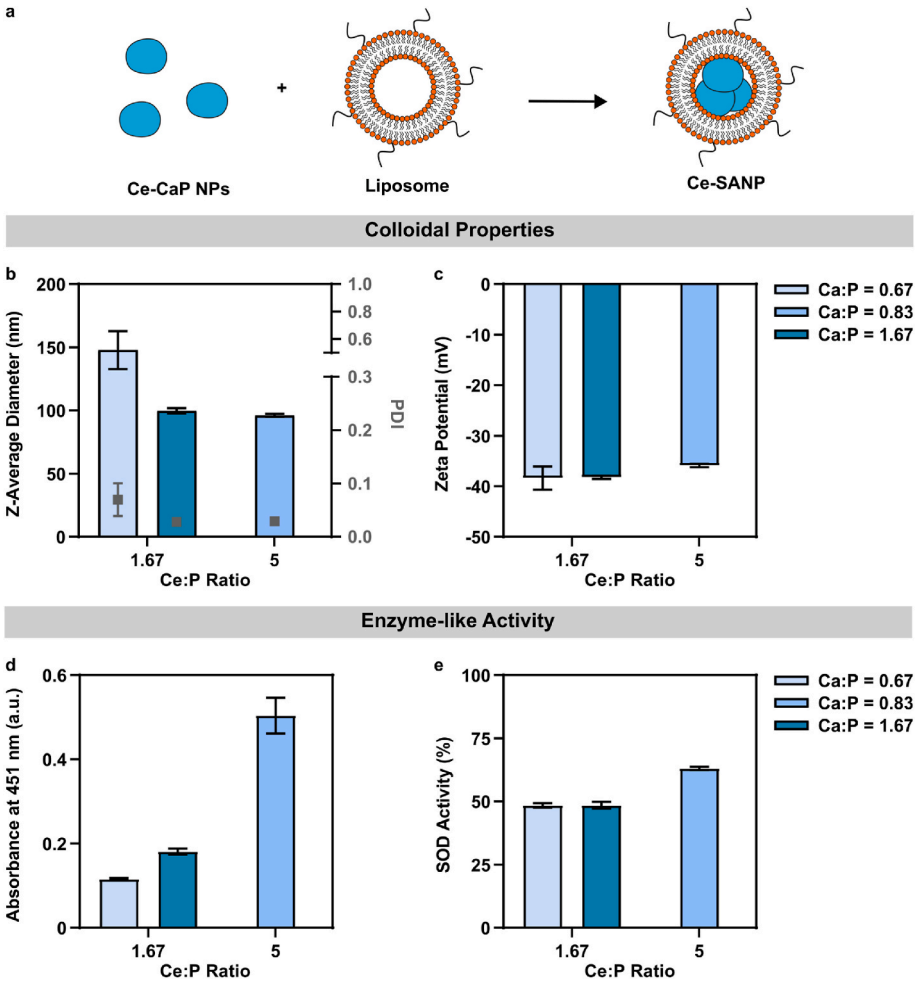

Fig. 5. Physico-chemical characterization of Ce-SANP. (a) Z-average diameter (bars), PDI (square symbols), and (b) zeta potential of Ce-SANP obtained by mixing cationic liposomes and Ce–CaP NPs with varying Ca:P and Ce:P ratios. Data is reported as mean ± s.d. of N = 2–3 independent batches. (c) Peroxidase-like activity of Ce-SANP with varying Ca:P and Ce:P ratios at 105 μg/mL (d) SOD-like activity of Ce-SANP with varying Ca:P and Ce:P ratios at 25 μg/mL. Data is reported as mean ± s.d. of N = 2–3 independent batches with n = 3 technical replicates.

cationic liposomes and Ce–CaP NPs with a Ce:P = 1.67 and Ca:P = 0.67 30 min post incubation at 37 °C, which is indicative of poor colloidal stability in both the NaCl and BSA solutions (Fig. 6). Negligible changes in the hydrodynamic diameter were observed for Ce-SANP formulations containing either Ce–CaP NPs with Ce:P = 1.67 and Ca:P = 1.67 or Ce–CaP NPs with Ce:P = 5 and Ca:P = 0.83, suggesting that these formulations may be suitable for intravenous administration.

It is worth mentioning that while we included a PEGylated lipid (Cer_{16}-PEG_{2000}) in the nanoparticle formulation to ensure the colloidal stability of the nanoparticles, PEG-based surfactants may be prone to auto-oxidation reactions [57]. This aspect has been recently investigated by Friedl and co-workers, who determined the hydroperoxide and aldehyde content upon UV-B irradiation of PEG-, polyglycerol (PG)-, and saccharide-based surfactants used as stabilizers in nanoparticle formulations [57]. Although auto-oxidation reactions for Cer_{16}-PEG_{2000} have not been investigated, a future perspective of this study could be the determination of its tendency to undergo auto-oxidation reactions and consider alternative surfactants with a reduced tendency to form hydroperoxides.

3.5. Cell viability and ROS-scavenging activity of Ce–CaP SANP formulations

For *in vitro* studies, we chose HepG2 cell line since it represents the most common model to evaluate drug metabolism and toxicity with high similarity to primary human hepatocytes [58–60]. Moreover, it is an appropriate tool to determine oxidative stress and related mitochondrial dysfunction [61]. Here, we first showed that Ce–CaP SANP formulations did not affect cell viability at the range of tested concentrations (30–300 μg/mL) after 24 h of treatment, regardless of the Ca:P and Ce:P ratios (Fig. 7).

Therefore, we evaluated the effect of the cerium-based NPs on oxidative damage induced in HepG2 by a pro-oxidant challenge. We demonstrated that all Ce–CaP SANPs markedly reduced ROS production in HepG2 cells in a concentration-dependent manner (Fig. 8), confirming the potential SOD-like activity of these formulations.

4. Conclusions

Here, we designed a self-assembling nanoparticle platform with antioxidant properties for ROS scavenging to limit oxidative damage in HepG2 cells. We modified the calcium phosphate core of the nanoparticles with cerium by preparing cerium-doped CaP NPs, whose hydrodynamic diameters and PDI were affected by the relative ratios between calcium, phosphate, and cerium. Most of the formulations exhibited good colloidal stability against aggregation for 21 days when stored at 4 °C, as well as upon reconstitution in water following lyophilization. The relative ratios among calcium, phosphate, and cerium could also dictate the peroxidase- and SOD-like activity of the cerium-doped CaP NPs. Mixing with cationic liposomes yielded cerium-doped SANP formulations, which exhibited z-average diameters < 150 nm, low PDI, and a negative surface charge. Cerium-doped SANP showed good stability against aggregation when incubated at 37 °C in the presence of serum proteins up to 4 h in a composition-dependent manner. The peroxidase- and SOD-like activity of the Ce–CaP NPs exhibited minimal variations upon mixing with the cationic liposomes. Cerium-doped SANP did not affect cell viability and reduced the ROS production in a concentration-dependent manner in HepG2 cells exposed to H_2O_2 as oxidative stressor. Future studies will be focused on loading the cerium-doped SANP formulations with RNA-based and/or conventional drugs used for the treatment of chronic liver diseases to evaluate *in vitro* and *in vivo* the potential of several multi-modal therapies.

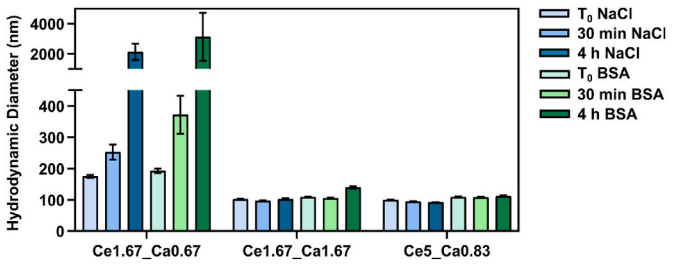

Fig. 6. Stability against aggregation of Ce-SANP formulations following dilution in 150 mM NaCl or BSA solution. Sample Ce1.67_Ca0.67 refers to formulations with Ce:P = 1.67 and Ca:P = 0.67, sample Ce1.67_Ca1.67 refers to formulations with Ce:P = 1.67 and Ca:P = 1.67, while sample Ce5_Ca0.83 refers to formulations with Ce:P = 5 and Ca:P = 0.83. Data are represented as mean ± s.d. (N = 2–3 independent batches, n = 2 technical replicates per batch).

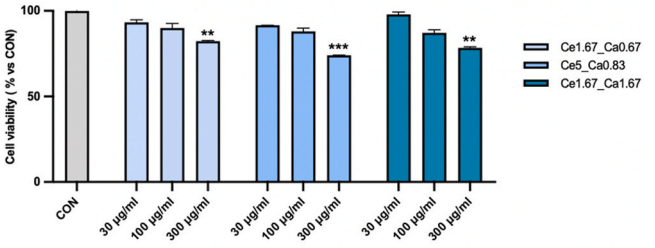

Fig. 7. Cell viability of HepG2 cells in presence or not of Ce–CaP SANP formulations at three different concentration (30–300 μM) for 24 h was assessed by MTT assay. Data are presented as presented as mean value ± SEM for at least three experiments. Differences among groups were considered significant at values of **P < 0.01, ***P < 0.001.

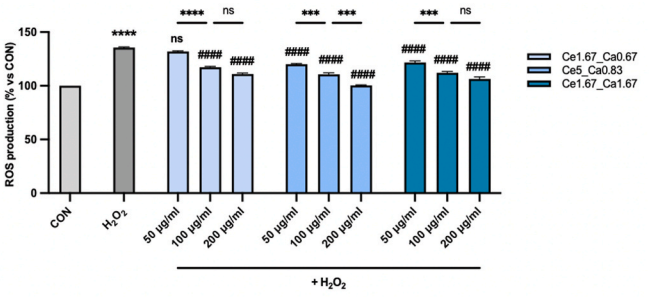

Fig. 8. The SOD-like activity of Ce–CaP SANP formulations on ROS production was evaluated using DCFH-DA assay. Data are presented as presented as mean value ± SEM for at least three experiments. Differences among groups were considered significant at values of ***P < 0.001, ****P < 0,0001 vs CON, $^{\#\#\#\#}$P < 0.0001 vs H_2O_2.

CRediT authorship contribution statement

Valeria Nele: Conceptualization, Data curation, Formal analysis, Investigation, Methodology, Visualization, Writing – original draft, Writing – review & editing. **Stefania Melini:** Formal analysis, Investigation, Methodology. **Virginia Campani:** Visualization, Writing – review & editing. **Alessia Angelillo:** Validation. **Sossio Fabio Graziano:** Formal analysis, Investigation, Methodology. **Claudio Pirozzi:** Formal analysis, Investigation, Methodology. **Rosaria Meli:** Funding acquisition, Project administration, Resources, Supervision. **Giuseppe De Rosa:** Conceptualization, Funding acquisition, Project administration, Resources, Supervision.

Declaration of competing interest

The authors declare that they have no known competing financial

interests or personal relationships that could have appeared to influence the work reported in this paper.

Data availability

Data will be made available on request.

Acknowledgements

V.N. was supported by Fondazione Umberto Veronesi Post-Doctoral Fellowship. We kindly acknowledge Dr. Roberto De Gennaro for the assistance with the SEM-EDS analysis and the use of microscopy facilities within of the Department of Earth Sciences, Environment and Resources, University of Naples Federico II. R.M. and G.D.R. acknowledge the grant CN00000041 ″National Center for Gene Therapy and Drugs based on RNA Technology" (Spoke 9 and Spoke 3, concession number 1035 of 17 June 2022-PNRR MUR - M4C2 - Investment 1.4 Call "National Centers", financed by EU- NextGenerationEU), project code (CUP E63C22000940007).

Appendix A. Supplementary data

Supplementary data to this article can be found online at https://doi.org/10.1016/j.jddst.2024.105490.

References

[1] A. Allameh, R. Niayesh-Mehr, A. Aliarab, G. Sebastiani, K. Pantopoulos, Oxidative stress in liver pathophysiology and disease, Antioxidants 12 (2023) 1653, https://doi.org/10.3390/antiox12091653.
[2] E.M. Brunt, V.W.-S. Wong, V. Nobili, C.P. Day, S. Sookoian, J.J. Maher, E. Bugianesi, C.B. Sirlin, B.A. Neuschwander-Tetri, M.E. Rinella, Nonalcoholic fatty liver disease, Nat. Rev. Dis. Prim. 1 (2015) 15080, https://doi.org/10.1038/nrdp.2015.80.
[3] J.C. Arroyave-Ospina, Z. Wu, Y. Geng, H. Moshage, Role of oxidative stress in the pathogenesis of non-alcoholic fatty liver disease: implications for prevention and therapy, Antioxidants 10 (2021) 174, https://doi.org/10.3390/antiox10020174.
[4] N.E. Sunny, F. Bril, K. Cusi, Mitochondrial adaptation in nonalcoholic fatty liver disease: novel mechanisms and treatment strategies, Trends Endocrinol. Metabol. 28 (2017) 250–260, https://doi.org/10.1016/j.tem.2016.11.006.
[5] S. Albhaisi, M. Noureddin, Current and potential therapies targeting inflammation in NASH, Front. Endocrinol. 12 (2021), https://doi.org/10.3389/fendo.2021.767314.
[6] J.H. Yang, S.C. Kim, K.M. Kim, C.H. Jang, S.S. Cho, S.J. Kim, S.K. Ku, I.J. Cho, S. H. Ki, Isorhamnetin attenuates liver fibrosis by inhibiting TGF-β/Smad signaling and relieving oxidative stress, Eur. J. Pharmacol. 783 (2016) 92–102, https://doi.org/10.1016/j.ejphar.2016.04.042.
[7] A. Gillessen, H.H.-J. Schmidt, Silymarin as supportive treatment in liver diseases: a narrative review, Adv. Ther. 37 (2020) 1279–1301, https://doi.org/10.1007/s12325-020-01251-y.
[8] H. Sebai, M. Sani, M.T. Yacoubi, E. Aouani, N. Ghanem-Boughanmi, M. Ben-Attia, Resveratrol, a red wine polyphenol, attenuates lipopolysaccharide-induced oxidative stress in rat liver, Ecotoxicol. Environ. Saf. 73 (2010) 1078–1083, https://doi.org/10.1016/j.ecoenv.2009.12.031.
[9] M.G. Traber, J.F. Stevens, Vitamins C and E: beneficial effects from a mechanistic perspective, Free Radic. Biol. Med. 51 (2011) 1000–1013, https://doi.org/10.1016/j.freeradbiomed.2011.05.017.
[10] V.N. Hieu, L.T.T. Thuy, H. Hai, N.Q. Dat, D.V. Hoang, N.V. Hanh, D.M. Phuong, T. H. Hoang, H. Sawai, Y. Shiro, M. Sato-Matsubara, D. Oikawa, F. Tokunaga, K. Yoshizato, N. Kawada, Capacity of extracellular globins to reduce liver fibrosis via scavenging reactive oxygen species and promoting MMP-1 secretion, Redox Biol. 52 (2022) 102286, https://doi.org/10.1016/j.redox.2022.102286.
[11] H. Hashemzadeh, M.Y. Hanafi-Bojd, M. Iranshahy, A. Zarban, H. Raissi, The combination of polyphenols and phospholipids as an efficient platform for delivery of natural products, Sci. Rep. 13 (2023) 2501, https://doi.org/10.1038/s41598-023-29237-0.
[12] A. Sadžak, M. Eraković, S. Šegota, Kinetics of flavonoid degradation and controlled release from functionalized magnetic nanoparticles, Mol. Pharm. (2023), https://doi.org/10.1021/acs.molpharmaceut.3c00478.
[13] A.C. Caritá, B. Fonseca-Santos, J.D. Shultz, B. Michniak-Kohn, M. Chorilli, G. R. Leonardi, Vitamin C: one compound, several uses. Advances for delivery, efficiency and stability, Nanomedicine 24 (2020) 102117, https://doi.org/10.1016/j.nano.2019.102117.
[14] C.-W. Li, L.-L. Li, S. Chen, J.-X. Zhang, W.-L. Lu, Antioxidant nanotherapies for the treatment of inflammatory diseases, Front. Bioeng. Biotechnol. 8 (2020), https://doi.org/10.3389/fbioe.2020.00200.
[15] A. Maqsoudlou, E. Assadpour, H. Mohebodini, S.M. Jafari, Improving the efficiency of natural antioxidant compounds via different nanocarriers, Adv. Colloid Interface Sci. 278 (2020) 102122, https://doi.org/10.1016/j.cis.2020.102122.
[16] E. Abbasi, S.A. Vafaei, N. Naseri, A. Darini, M.T. Azandaryani, F.K. Ara, F. Mirzaei, Protective effects of cerium oxide nanoparticles in non-alcoholic fatty liver disease (NAFLD) and carbon tetrachloride-induced liver damage in rats: study on intestine and liver, Metabol Open 12 (2021) 100151, https://doi.org/10.1016/j.metop.2021.100151.
[17] S. Carvajal, M. Perramón, D. Oró, E. Casals, G. Fernández-Varo, G. Casals, M. Parra, B. González de la Presa, J. Ribera, Ó. Pastor, M. Morales-Ruíz, V. Puntes, W. Jiménez, Cerium oxide nanoparticles display antilipogenic effect in rats with non-alcoholic fatty liver disease, Sci. Rep. 9 (2019) 12848, https://doi.org/10.1038/s41598-019-49262-2.
[18] G. Casals, M. Perramón, E. Casals, I. Portolés, G. Fernández-Varo, M. Morales-Ruiz, V. Puntes, W. Jiménez, Cerium oxide nanoparticles: a new therapeutic tool in liver diseases, Antioxidants 10 (2021) 660, https://doi.org/10.3390/antiox10050660.
[19] T. Yang, M. Poenisch, R. Khanal, Q. Hu, Z. Dai, R. Li, G. Song, Q. Yuan, Q. Yao, X. Shen, R. Taubert, B. Engel, E. Jaeckel, A. Vogel, C.S. Falk, A. Schambach, D. Gerovska, M.J. Araúzo-Bravo, F.W.R. Vondran, T. Cantz, N. Horscroft, A. Balakrishnan, F. Chevessier, M. Ott, A.D. Sharma, Therapeutic HNF4A mRNA attenuates liver fibrosis in a preclinical model, J. Hepatol. 75 (2021) 1420–1433, https://doi.org/10.1016/j.jhep.2021.08.011.
[20] Z. Zhao, C.-Y. Lin, K. Cheng, siRNA- and miRNA-based therapeutics for liver fibrosis, Transl. Res. 214 (2019) 17–29, https://doi.org/10.1016/j.trsl.2019.07.007.
[21] T.C. Roberts, R. Langer, M.J.A. Wood, Advances in oligonucleotide drug delivery, Nat. Rev. Drug Discov. 19 (2020) 673–694, https://doi.org/10.1038/s41573-020-0075-7.
[22] G. Salzano, M. Marra, M. Porru, S. Zappavigna, A. Abbruzzese, M.I. La Rotonda, C. Leonetti, M. Caraglia, G. De Rosa, Self-assembly nanoparticles for the delivery of bisphosphonates into tumors, Int. J. Pharm. 403 (2011) 292–297, https://doi.org/10.1016/j.ijpharm.2010.10.046.
[23] M. Porru, S. Zappavigna, G. Salzano, A. Luce, A. Stoppacciaro, M.L. Balestrieri, S. Artuso, S. Lusa, G. De Rosa, C. Leonetti, M. Caraglia, Medical treatment of orthotopic glioblastoma with transferrin-conjugated nanoparticles encapsulating zoledronic acid, Oncotarget 5 (No 21) (2014) 10446, https://doi.org/10.18632/oncotarget.2182.
[24] G. Salzano, S. Zappavigna, A. Luce, N. D'Onofrio, M.L. Balestrieri, A. Grimaldi, S. Lusa, D. Ingrosso, S. Artuso, M. Porru, C. Leonetti, M. Caraglia, G. De Rosa, Transferrin-targeted nanoparticles containing zoledronic acid as a potential tool to inhibit glioblastoma growth, J. Biomed. Nanotechnol. 12 (2016) 811–830, https://doi.org/10.1166/jbn.2016.2214.
[25] M. Marra, G. Salzano, C. Leonetti, M. Porru, R. Franco, S. Zappavigna, G. Liguori, G. Botti, P. Chieffi, M. Lamberti, G. Vitale, A. Abbruzzese, M.I. La Rotonda, G. De Rosa, M. Caraglia, New self-assembly nanoparticles and stealth liposomes for the delivery of zoledronic acid: a comparative study, Biotechnol. Adv. 30 (2012) 302–309, https://doi.org/10.1016/j.biotechadv.2011.06.018.
[26] V. Campani, S. Zappavigna, L. Scotti, M. Abate, M. Porru, C. Leonetti, M. Caraglia, G. De Rosa, Hybrid lipid self-assembling nanoparticles for brain delivery of microRNA, Int. J. Pharm. 588 (2020) 119693, https://doi.org/10.1016/j.ijpharm.2020.119693.
[27] V. Nele, V. Tedeschi, V. Campani, R. Ciancio, A. Angelillo, S.F. Graziano, G. De Rosa, A. Secondo, Cerium-doped self-assembling nanoparticles as a novel antioxidant delivery system preserving mitochondrial function in cortical neurons exposed to ischemia-like conditions, Antioxidants 12 (2023), https://doi.org/10.3390/antiox12020358.
[28] C. Rispoli, A. De Bonis, V. Guarino, S.F. Graziano, C. Di Benedetto, R. Esposito, V. Morra, P. Cappelletti, The ancient pozzolanic mortars of the Thermal complex of Baia (Campi Flegrei, Italy), J. Cult. Herit. 40 (2019) 143–154, https://doi.org/10.1016/j.culher.2019.05.010.
[29] C. Qiu, Y. Wu, Q. Guo, Q. Shi, J. Zhang, Y. Meng, F. Xia, J. Wang, Preparation and application of calcium phosphate nanocarriers in drug delivery, Mater Today Bio 17 (2022) 100501, https://doi.org/10.1016/j.mtbio.2022.100501.
[30] A.-Y. Cai, Y.-J. Zhu, C. Qi, Biodegradable inorganic nanostructured biomaterials for drug delivery, Adv. Mater. Interfac. 7 (2020) 2000819, https://doi.org/10.1002/admi.202000819.
[31] M.A. Khan, V.M. Wu, S. Ghosh, V. Uskoković, Gene delivery using calcium phosphate nanoparticles: optimization of the transfection process and the effects of citrate and poly(l -lysine) as additives, J. Colloid Interface Sci. 471 (2016) 48–58, https://doi.org/10.1016/j.jcis.2016.03.007.
[32] V. di Mauro, M. Iafisco, N. Salvarani, M. Vacchiano, P. Carullo, G.B. Ramírez-Rodríguez, T. Patrício, A. Tampieri, M. Miragoli, D. Catalucci, Bioinspired negatively charged calcium phosphate nanocarriers for cardiac delivery of MicroRNAs, Nanomedicine 11 (2016) 891–906, https://doi.org/10.2217/nnm.16.26.
[33] Y. Kakizawa, S. Furukawa, K. Kataoka, Block copolymer-coated calcium phosphate nanoparticles sensing intracellular environment for oligodeoxynucleotide and siRNA delivery, J. Contr. Release 97 (2004) 345–356, https://doi.org/10.1016/j.jconrel.2004.03.031.
[34] X. Huang, D. Andina, J. Ge, A. Labarre, J.-C. Leroux, B. Castagner, Characterization of calcium phosphate nanoparticles based on a PEGylated chelator for gene delivery, ACS Appl. Mater. Interfaces 9 (2017) 10435–10445, https://doi.org/10.1021/acsami.6b15925.
[35] H. Urch, M. Vallet-Regi, L. Ruiz, J.M. Gonzalez-Calbet, M. Epple, Calcium phosphate nanoparticles with adjustable dispersability and crystallinity, J. Mater. Chem. 19 (2009) 2166, https://doi.org/10.1039/b810026h.

[36] J. Klesing, A. Wiehe, B. Gitter, S. Gräfe, M. Epple, Positively charged calcium phosphate/polymer nanoparticles for photodynamic therapy, J. Mater. Sci. Mater. Med. 21 (2010) 887–892, https://doi.org/10.1007/s10856-009-3934-7.
[37] Y.-Y. Hu, A. Rawal, K. Schmidt-Rohr, Strongly bound citrate stabilizes the apatite nanocrystals in bone, Proc. Natl. Acad. Sci. USA 107 (2010) 22425–22429, https://doi.org/10.1073/pnas.1009219107.
[38] L. Degli Esposti, A. Adamiano, D. Siliqi, C. Giannini, M. Iafisco, The effect of chemical structure of carboxylate molecules on hydroxyapatite nanoparticles. A structural and morphological study, Bioact. Mater. 6 (2021) 2360–2371, https://doi.org/10.1016/j.bioactmat.2021.01.010.
[39] A. Adamiano, M. Iafisco, M. Sandri, M. Basini, P. Arosio, T. Canu, G. Sitia, A. Esposito, V. Iannotti, G. Ausanio, E. Fragogeorgi, M. Rouchota, G. Loudos, A. Lascialfari, A. Tampieri, On the use of superparamagnetic hydroxyapatite nanoparticles as an agent for magnetic and nuclear in vivo imaging, Acta Biomater. 73 (2018) 458–469, https://doi.org/10.1016/j.actbio.2018.04.040.
[40] P. Mi, D. Kokuryo, H. Cabral, H. Wu, Y. Terada, T. Saga, I. Aoki, N. Nishiyama, K. Kataoka, A pH-activatable nanoparticle with signal-amplification capabilities for non-invasive imaging of tumour malignancy, Nat. Nanotechnol. 11 (2016) 724–730, https://doi.org/10.1038/nnano.2016.72.
[41] N. Yang, S. Wang, P. Ding, S. Sun, Q. Wei, H. Jafari, L. Wang, Y. Han, O.V. Okoro, T. Wang, G. Li, A. Shavandi, L. Nie, Magnesium-doped biphasic calcium phosphate nanoparticles with incorporation of silver: synthesis, cytotoxic and antibacterial properties, Mater. Lett. 322 (2022) 132478, https://doi.org/10.1016/j.matlet.2022.132478.
[42] G. Vinothkumar, A.I. Lalitha, K. Suresh Babu, Cerium phosphate–cerium oxide heterogeneous composite nanozymes with enhanced peroxidase-like biomimetic activity for glucose and hydrogen peroxide sensing, Inorg. Chem. 58 (2019) 349–358, https://doi.org/10.1021/acs.inorgchem.8b02423.
[43] M.L. Hancock, R.A. Yokel, M.J. Beck, J.L. Calahan, T.W. Jarrells, E.J. Munson, G. A. Olaniyan, E.A. Grulke, The characterization of purified citrate-coated cerium oxide nanoparticles prepared via hydrothermal synthesis, Appl. Surf. Sci. 535 (2021) 147681, https://doi.org/10.1016/j.apsusc.2020.147681.
[44] Y. Yang, Z. Mao, W. Huang, L. Liu, J. Li, J. Li, Q. Wu, Redox enzyme-mimicking activities of CeO2 nanostructures: intrinsic influence of exposed facets, Sci. Rep. 6 (2016) 35344, https://doi.org/10.1038/srep35344.
[45] W. Wang, X. Jiang, K. Chen, CePO4:Tb,Gd hollow nanospheres as peroxidase mimic and magnetic–fluorescent imaging agent, Chem. Commun. 48 (2012) 6839, https://doi.org/10.1039/c2cc32328a.
[46] N. Alizadeh, A. Salimi, T.-K. Sham, P. Bazylewski, G. Fanchini, Intrinsic enzyme-like activities of cerium oxide nanocomposite and its application for extracellular H $_2$ O $_2$ detection using an electrochemical microfluidic device, ACS Omega 5 (2020) 11883–11894, https://doi.org/10.1021/acsomega.9b03252.
[47] V. Baldim, F. Bedioui, N. Mignet, I. Margaill, J.-F. Berret, The enzyme-like catalytic activity of cerium oxide nanoparticles and its dependency on Ce $^{3+}$ surface area concentration, Nanoscale 10 (2018) 6971–6980, https://doi.org/10.1039/C8NR00325D.
[48] G. Kignelman, S. Eyley, C. Zhou, B. Tunca, M. Gonon, D. Lahem, J.W. Seo, W. Thielemans, Colloidal stability and aggregation mechanism in aqueous suspensions of TiO $_2$ nanoparticles prepared by sol–gel synthesis, Langmuir 37 (2021) 14846–14855, https://doi.org/10.1021/acs.langmuir.1c02533.
[49] A. Asati, S. Santra, C. Kaittanis, S. Nath, J.M. Perez, Oxidase-like activity of polymer-coated cerium oxide nanoparticles, Angew. Chem. Int. Ed. 48 (2009) 2308–2312, https://doi.org/10.1002/anie.200805279.
[50] A. Asati, S. Santra, C. Kaittanis, J.M. Perez, Surface-charge-dependent cell localization and cytotoxicity of cerium oxide nanoparticles, ACS Nano 4 (2010) 5321–5331, https://doi.org/10.1021/nn100816s.
[51] M.S. Lord, B. Tsoi, C. Gunawan, W.Y. Teoh, R. Amal, J.M. Whitelock, Anti-angiogenic activity of heparin functionalised cerium oxide nanoparticles, Biomaterials 34 (2013) 8808–8818, https://doi.org/10.1016/j.biomaterials.2013.07.083.
[52] G. Goujon, V. Baldim, C. Roques, N. Bia, J. Seguin, B. Palmier, A. Graillot, C. Loubat, N. Mignet, I. Margaill, J. Berret, V. Beray-Berthat, Antioxidant activity and toxicity study of cerium oxide nanoparticles stabilized with innovative functional copolymers, Adv. Healthcare Mater. 10 (2021) 2100059, https://doi.org/10.1002/adhm.202100059.
[53] J.-F. Berret, A. Graillot, Versatile coating platform for metal oxide nanoparticles: applications to materials and biological science, Langmuir 38 (2022) 5323–5338, https://doi.org/10.1021/acs.langmuir.2c00338.
[54] N. Pramanik, T. De, P. Sharma, A. Alakesh, S.K. Jagirdar, A. Rangarajan, S. Jhunjhunwala, Surface-coated cerium nanoparticles to improve chemotherapeutic delivery to tumor cells, ACS Omega 7 (2022) 31651–31657, https://doi.org/10.1021/acsomega.2c00062.
[55] S. Ristori, I. Grillo, S. Lusa, J. Thamm, G. Valentino, V. Campani, M. Caraglia, F. Steiniger, P. Luciani, G. De Rosa, Structural characterization of self-assembling hybrid nanoparticles for bisphosphonate delivery in tumors, Mol. Pharm. 15 (2018) 1258–1265, https://doi.org/10.1021/acs.molpharmaceut.7b01085.
[56] B.G. Cha, H.-G. Jeong, D.-W. Kang, M.-J. Nam, C.K. Kim, D.Y. Kim, I.-Y. Choi, S. K. Ki, S.I. Kim, J. hee Han, J. Kim, S.-H. Lee, Customized lipid-coated magnetic mesoporous silica nanoparticle doped with ceria nanoparticles for theragnosis of intracerebral hemorrhage, Nano Res. 11 (2018) 3582–3592, https://doi.org/10.1007/s12274-017-1924-5.
[57] J. David Friedl, R. Wibel, Z. Burcu Akkuş-Dağdeviren, A. Bernkop-Schnürch, Reactive oxygen species (ROS) in colloidal systems: are “PEG-free” surfactants the answer? J. Colloid Interface Sci. 616 (2022) 571–583, https://doi.org/10.1016/j.jcis.2022.02.092.
[58] C. Pirozzi, A. Lama, C. Annunziata, G. Cavaliere, C. De Caro, R. Citraro, E. Russo, M. Tallarico, M. Iannone, M.C. Ferrante, M.P. Mollica, G. Mattace Raso, G. De Sarro, A. Calignano, R. Meli, Butyrate prevents valproate-induced liver injury: in vitro and in vivo evidence, Faseb. J. 34 (2020) 676–690, https://doi.org/10.1096/fj.201900927RR.
[59] M. Ruoß, G. Damm, M. Vosough, L. Ehret, C. Grom-Baumgarten, M. Petkov, S. Naddalin, R. Ladurner, D. Seehofer, A. Nussler, S. Sajadian, Epigenetic modifications of the liver tumor cell line HepG2 increase their drug metabolic capacity, Int. J. Mol. Sci. 20 (2019), https://doi.org/10.3390/ijms20020347.
[60] N.T.T. Tham, S.-R. Hwang, J.-H. Bang, H. Yi, Y.-I. Park, S.-J. Kang, H.-G. Kang, Y.-S. Kim, H.-O. Ku, High-content analysis of in vitro hepatocyte injury induced by various hepatotoxicants, J. Vet. Sci. 20 (2019) 34–42, https://doi.org/10.4142/jvs.2019.20.1.34.
[61] L. Tolosa, N. Jiménez, G. Pérez, J. V Castell, M.J. Gómez-Lechón, M.T. Donato, Customised in vitro model to detect human metabolism-dependent idiosyncratic drug-induced liver injury, Arch. Toxicol. 92 (2018) 383–399, https://doi.org/10.1007/s00204-017-2036-4.